Contents lists available at ScienceDirect

Applied Catalysis B: Environmental

journal homepage: http://ees.elsevier.com

All-organic Z-scheme photoreduction of CO_2 with water as the donor of electrons and protons

Stefano Mazzanti [a], Shaowen Cao [a,b], Katharina ten Brummelhuis [a], Antje Völkel [a], Jagadish Khamrai [c], Dmitry I. Sharapa [d], Sol Youk [a], Tobias Heil [a], Nadezda V. Tarakina [a], Volker Strauss [a], Indrajit Ghosh [c], Burkhard König [c], Martin Oschatz [a], Markus Antonietti [a], Aleksandr Savateev [a,*]

[a] Max-Planck Institute of Colloids and Interfaces, Department of Colloid Chemistry, Research Campus Golm, Am Mühlenberg 1, 14476 Potsdam, Germany
[b] State Key Laboratory of Advanced Technology for Materials Synthesis and Processing, Wuhan University of Technology, 122 Luoshi Road, Wuhan 430070, PR China
[c] Fakultät für Chemie und Pharmazie, Universität Regensburg, 93040 Regensburg, Germany
[d] Institute of Catalysis Research and Technology, Karlsruhe Institute of Technology (KIT), Herrmann-von-Helmholtz-Platz 1, 76344 Eggenstein-Leopoldshafen, Germany

ARTICLE INFO

Keywords
Carbon nitride
Photocatalysis
CO_2
Flavins
Heterojunctions

ABSTRACT

Carbon nitrides and flavins are two classes of easy accessible transition metal-free, photoactive materials. Their photocatalytic efficiency to enable a variety of chemical reactions is well documented. Here, we report on their combination in one photocatalytic system by designing biomimetic non-spherical core-shell architectures comprising micro-sized crystals of flavins decorated by potassium poly(heptazine imide) nanoparticles on the surface. The designed non-spherical core-shell composites are tested in the photocatalytic CO_2 reduction to CH_4, MeOH, EtOH and CO using water vapor as a donor of electrons and protons at the gas-solid interface. The forged Z-scheme heterojunction between these two materials allows increasing of their photocatalytic performance. Whereby excited states lifetimes are extended by interface charge recombination and photoredox processes are boosted because of an overall wider band gap.

1. Introduction

Extensive, anthropogenic combustion of fossil fuels into CO_2 is the main contributor to global warming [1] and artificial photosynthesis is considered as one of the most promising approaches to address the involved problems [2]. Previous research in artificial photosynthesis proved that a series of valuable chemicals, for example, CO [3], methanol [4], ethanol [5], can be prepared from CO_2 using synthetic materials as photocatalysts, while water is the most attractive donor of electrons and protons [6]. Many materials have been reported to promote CO_2 reduction under light irradiation [6], but limited stability and efficiency of the process limit applications [7].

Riboflavin (vitamin B2) and its derivatives are eco-friendly, cheap [8], non-toxic [9] redox active dyes. They have been employed mostly as homogeneous photocatalysts to perform photo-oxidations [8,10–17], but were also reported in heterogeneous photocatalysis, here supported on nanostructured metal oxide films for the oxidation of alkylbenzenes [12]. In addition, riboflavin tetrabutyrate was used as emission layer in OLEDs [18]. However, photocatalytic reduction reactions mediated by flavins have not been explored [19].

On the other hand the larger class of carbon nitride (CN) materials, after uprising in H_2 evolution under visible light, has been also applied in organic synthesis [20–28] and in solar energy storage applications [29]. Several methods have been developed to tune physical and chemical properties of CNs, and as a result, to enhance the photocatalytic activity in a certain reaction [30]. Band gap engineering is considered as a key strategy to tune CNs properties in a desirable way [29]. The following strategies are distinguished within this approach: 1) elemental and molecular doping of CNs [30], 2) supramolecular preorganization of monomers [31,32], 3) ionothermal synthesis, for example, in LiCl/KCl eutectics [31,33–35] and 4) construction of the heterojunctions, for example, with metal oxides like TiO_2 [36]. Finally, construction of donor-acceptor conjugated polymers has been widely used [37–40]. However, this last strategy has been seldom applied to CNs based material.

An electron deficient CN family member, potassium poly(heptazine imide) (K-PHI, Fig. 1), is characterized by highly positive potential of the valence band (+2.2 V vs NHE) and is thereby a promising candidate for construction of such donor-acceptor composites [22,33,40]. The features of K-PHI has been employed earlier, for example, in benzylic C—H thiolation of alkylbenzenes, in which oxidation of the or-

* Corresponding author.
E-mail address: oleksandr.savatieiev@mpikg.mpg.de (A. Savateev)

https://doi.org/10.1016/j.apcatb.2020.119773
Received 12 June 2020; Received in revised form 10 November 2020; Accepted 29 November 2020
Available online xxx
0926-3373/

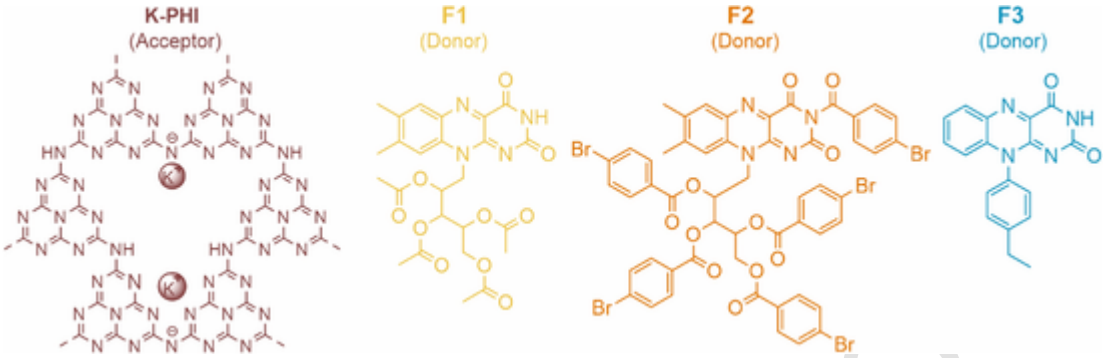

Fig. 1. Chemical structures of K-PHI and flavins employed in this work.

ganic substrate is a rate-limiting step [41]. The intrinsic (right after synthesis, without post treatment) morphology of K-PHI is featured by nanoparticles with an average diameter of 100 nm that gives higher surface-to-volume ratio compared to bulk carbon nitride materials represented by particles with few micrometers size [42]. The small particle size of K-PHI we consider as beneficial also to ensure a high interface area between two components when constructing heterogeneous donor-acceptor composites.

Herein, we bring the two classes of materials together – flavins and K-PHI to design donor-acceptor composites. In this approach K-PHI nanoparticles represent the acceptor, while flavins micro-sized crystals – the donor. This biomimetic architecture is tested in a gas-solid reactor to achieve CO_2 photoreduction using mere H_2O vapor as a source of electrons and protons, while oxygen is formed as the only other product. This kind of photocatalytic reactor allows convenient separation of the products from the catalyst without laborious workup and is to be seen as a set-up closest to scale up.

2. Experimental

2.1. Materials preparation

2.1.1. Preparation procedure and characterization of K-PHI

Preparation procedure and characterization of K-PHI) synthesis and characterization is in according to previous works [33,41,45–50].

2.1.2. Preparation of composites C1 (K-PHI/F-1 2:1), C2 (K-PHI/F-2 2:1), C3 (K-PHI/F-3 2:1)

In a flask (100 mL), flavin (0.1 mmol, 54.45 mg of F1 for C1, 129.14 mg of F2 for C2, 31.83 mg of F3 for C3) and K-PHI (0.2 mmol, 100 mg) were dissolved in methanol (25 mL). Suspension were stirred for 30 min. MeOH was evaporated, the solid was transferred into a mortar, grind it and the put into a porcelain crucible. Solids were heated at 150 ˚C for 6 h in oven in air.

2.2. Characterization of materials

2.2.1. Powder X-Ray diffraction patterns (PXRD)

Samples were measured on a Bruker D8 Advance diffractometer equipped with a scintillation counter detector with CuK_α radiation ($\lambda = 0.15418$ nm) applying 2θ step size of 0.05˚ and counting time of 3 s per step.

2.2.2. Scanning electron microscopy (SEM)

Sample images were obtained on a Zeiss LEO 1550-Gemini microscope.

2.2.3. Transmission electron microscopy (TEM)

For high-resolution transmission electron microscopy (HR-TEM) observations, samples were sonicated in ethanol for 10 min; the obtained suspensions were drop-casted to a Cu grid with a lacey carbon support and dried for 15 min. HRTEM studies were performed using a double Cs corrected JEOL JEM-ARM200 F (S)TEM operated at 80 kV, equipped with a cold-field emission gun, and a high-angle silicon drift Energy Dispersive X-ray (EDX) detector (solid angle up to 0.98 steradians with a detection area of 100 mm^2).

2.2.4. Optical absorbance spectra

Optical absorbance spectra of powders were measured on a Shimadzu UV 2600 equipped with an integrating sphere.

2.2.5. Emission spectra, Internal and External Quantum Efficiency (IQE/EQE)

Emission spectra, Internal and External Quantum Efficiency (IQE/EQE) were recorded on Jasco FP-8300 instrument. The excitation wavelength was set at 360 nm.

2.2.6. Thermal response measurements

Analysis were carried out by using an optical calorimeter (InfraSORP Technology by Fraunhofer/Rubotherm).

3. Results and discussion

The composites (C1, C2 and C3) self-assemble by in situ crystallization of the corresponding flavins (F1, F2 and F3, see Figs. S1–S2 for their preparation) from methanol solution upon concentration in vacuum followed by spontaneous deposition of K-PHI nanoparticles as a type of Pickering stabilizer (Fig. 2). The molar ratio between K-PHI and flavins has been chosen to 2:1 (assuming a repetitive molar weight of K-PHI of 500 g mol^{-1}) to ensure complete coverage of the flavin mi-

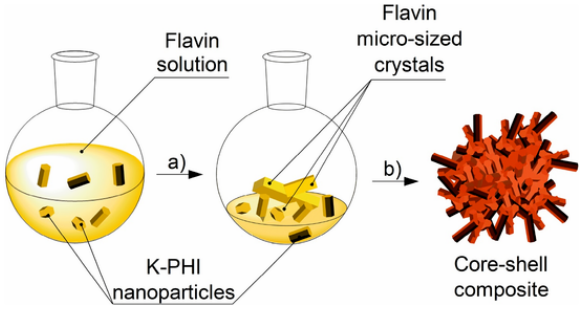

Fig. 2. Schematic procedure of non-spherical core-shell composite preparation and schematic representation of the composite morphology. Color staining of the composite illustrates red-shifted onset of light absorption in the heterojunction as evidenced by DRUV-vis spectroscopy (see below). Schematic representation of flavin and the non-spherical core-shell composite morphology as evidenced by the SEM images of flavin F3 and composite C3. Step a) denotes stirring a colloidal solution of K-PHI nanoparticles and flavin in MeOH followed by concentration under reduced pressure b) denotes grinding in mortar followed by annealing in air oven at 150 ˚C.

crocrystals with K-PHI nanoparticles and to achieve high interface area between the donor and acceptor in solid state.

Fig. 3 shows the morphology of flavins and the composites. The morphology of flavin F1 is represented by thin plates (Fig. 3a), flavin F2 by sharp-edged particles of irregular shape and flavin F3 by rectangular bricks. The SEM images of composites C1, C2 and C3 do not show morphological features of the pure flavins, but are rather identical to that of pure K-PHI – assembly of nanoparticles with the diameter 100−200 nm (see also Figs. S3–S9 for overview images), which means that flavin crystals are indeed completely covered by the PHI colloidal stabilizer. Thus, SEM provides the first piece of evidence that flavins and K-PHI form core-shell structures, albeit non-spherical, upon self-assembly – flavin crystals in the core, while the shell is constructed from K-PHI particles.

To get more insights about the structure of the obtained composites at the nanoscale we used transmission electron microscopy and energy-dispersive X-ray (EDX) analysis. The later allows clear distinguishing between deferent part of the composites, since bromine is present exclusively in flavin and potassium – in K-PHI. Fig. S10 shows a typical amorphous particle of flavin F2 with diameter of about 500 nm. In the corresponding C2 composite large amorphous particles of flavin F2 are decorated with nanocrystalline K-PHI nanoparticles (typically <100 nm in diameter) (Figs. 3g,h, S11) [42]. Analysis of HRTEM images and corresponding FFT transforms allows to conclude that formed K-PHI particles crystallize in hexagonal structure, with $a = 12.6$ Å, $c = 3.3$ Å (Fig. 3i-k) [43,44]. EDX spectra obtained from different parts of non-spherical core-shell structures have different K:Br ratios; thus crystalline parts exhibit a higher K content (Fig. S12c) while the amorphous part, the flavin-rich region, display a higher Br signal (Fig. S12f).

PXRD analysis of K-PHI nanoparticles reveals a typical pattern for this material with a pronounced peak at 8°, due to the in-plane periodicity, and the peak at 28° due to graphitic packing (Fig. S13a) [47]. Flavins F1 and F3 are crystalline powders, while F2 is amorphous (Fig. S13b, d, f). Higher crystallinity of flavins F1 and F3 is explained by a smaller and more regular shape of the molecule, i.e., a lower number of degrees of freedom that facilitates crystallization. Composites C1 and C2 are amorphous with respect to the flavin core, but all composites show pronounced peaks related to the presence of K-PHI nanoparticles (Fig. S13c, e, g), while intensity of the diffraction peaks depends of K-PHI content in the composites (Fig. S14, Table S1).

Fourier-transform infrared (FT-IR) spectra of the composites are very similar to that of K-PHI, while vibration peaks related to the flavins are mainly absent (Figs. 4 and S15). FT-IR data provide a second piece of evidence supporting the formation of the core-shell structure. In this architecture the flavin core is covered by the K-PHI shell. As a result, the vibrational peaks of the shell are predominantly seen in the IR spectra.

The solid-state emission spectra of the flavins, K-PHI and their composites are shown in Figs. 5a and S16. Pure flavins have fluorescence Internal Quantum Efficiency (IQE) 2.0–7.7 %, while K-PHI has an IQE of 0.19 % (Table S2). Practically complete fluorescence quenching is observed for composites in the solid state – composites IQEs are only 0.1-0.4 % (Table S2). Titration experiments showed that the composite with only 9 % K-PHI content already shows complete fluorescence quenching (Fig. 5c). These results give a third piece of evidence supporting formation of an electronically active structure. Taking into account results of the electron microscopy study and FT-IR, electronic interaction between the partners of the composite is obviously the most efficient when they are assembled in core-shell structure. A similar behavior has been reported for flavin-graphene composites [51].

However, dispersions of the composites C1 and C3 in DMSO *d*o not exhibit fluorescence quenching (Fig. S17) suggesting that polar solvent

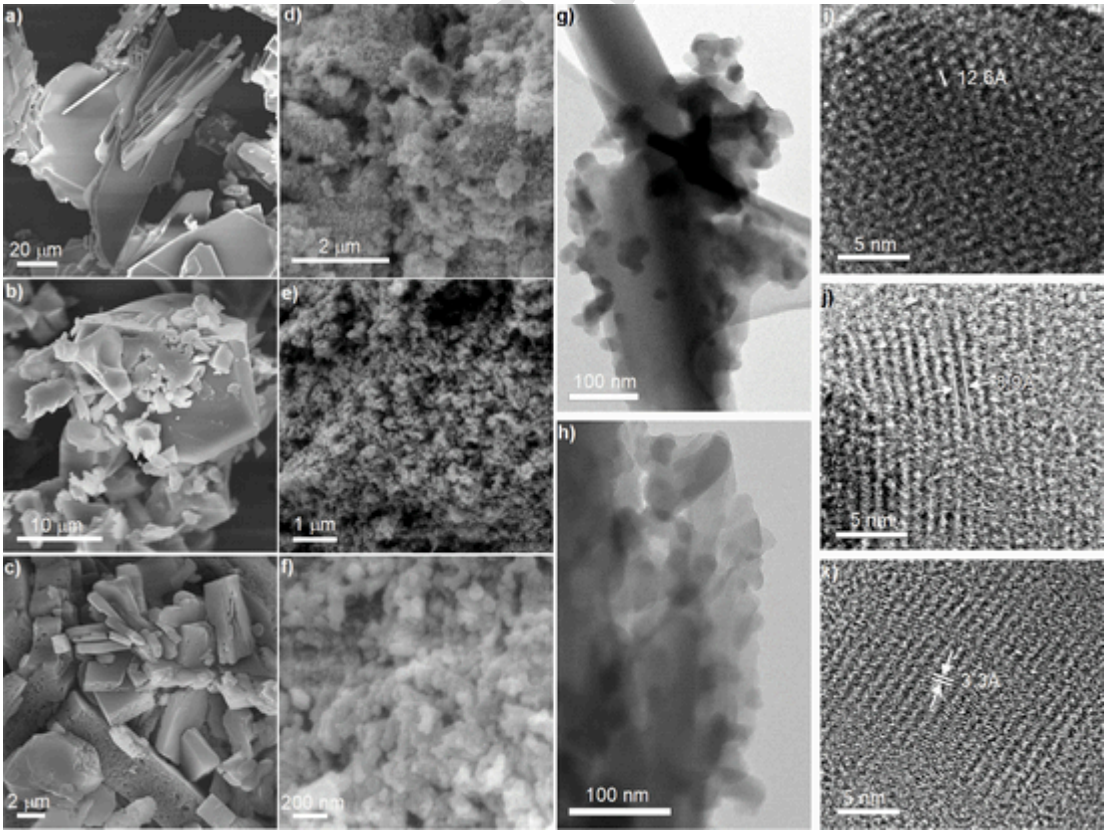

Fig. 3. Electron microscopy images of the flavins and their composites. SEM images of: a) Flavine F1; b) Flavine F2; c) Flavine F3; d) Composite C1; e) Composite C2; f) Composite C3; g,h) overview TEM images of the composite C2. i,j,k) HR-TEM images of K-PHI nanoparticles in the composite C2 taken along different crystallographic directions.

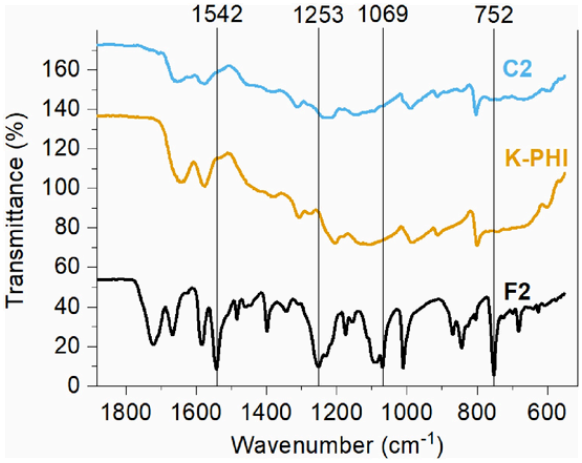

Fig. 4. FT-IR spectra of flavin F1, K-PHI and composite C1 in comparison. Selected vibrational peaks of flavin are labeled.

disrupts the interaction between the flavins F1 and F3 and K-PHI particles. In addition, dispersion of the composite C1 in DMSO followed by filtration, resulted in yellowish solution, implying dissolution of the flavin F1 in DMSO (Fig. S18). Furthermore, IQE of a series of K-PHI/F1 mixtures in DMSO with different K-PHI content shows an opposite trend compared to the measurements in solid state (Fig. 5c), i.e. higher IQE (8.5 %) for pure K-PHI suspension. On the other hand, flavin F1 showed lower IQE (2.2 %) compared to that in solid state (7.7 %), which is explained by an agglomeration induced emission phenomenon [52]. Since in the present work we apply the synthesized composites in the photocatalytic CO_2 reduction in the gas-solid interface, we consider spectroscopic data obtained in the solid state to be more relevant to the study.

Thermogravimetric analysis (TGA) of the C2 demonstrates lower mass loss in the composite compared to the calculated value, suggesting that the shell made of thermodynamically stable K-PHI nanoparticles stabilizes flavin core in the composite (Fig. S19). Overall, observation of the composites morphology directly from the electron microscopy images, FT-IR data, strong fluorescence quenching in the composites and TGA data, collectively support formation of non-spherical core-shell structures.

In agreement with earlier reports, K-PHI has an onset of absorption at 700 nm that is assigned to n-π* transitions [53], but the main contribution to light absorption originates from the π-π* transitions observed as a band at 460 nm, i.e., the band gap, as concluded from the diffuse reflectance (DR) UV–vis absorption spectra (Fig. 5d). In the solid state, all flavins have the onset of absorption at 540 nm that corresponds to the optical band gap of ca. 2.3 eV (Fig. S20). Similar band gap values of flavins, despite different backbone structure, i.e. protected ribose backbone (in case of F1 and F2) and 4-ethylphenyl substituent (in F3), support the fact that the isoalloxazine core acts as the chromophore.

Band gap values derived from the DRUV-vis spectra are close to that obtained from the cyclic voltammetry (CV) measurements of the flavins in MeCN solution, 2.27–2.34 eV (Fig. 5e). Considering the relative alignment of the frontier orbitals energy levels in flavins and CB/VB energy levels in K-PHI (Fig. 5f), the designed composites can be regarded as being able to follow a Z-scheme activation, if we make a comparison with all-semiconductor systems [54]. The Z-scheme rationalizes the complete fluorescence quenching observed in the composites in the solid state. Indeed, this is due to the selective charge recombination at the interface, while energy transfer is suppressed, as already reported for a flavin-graphene composite [51] and for a carbon nitride-carbon composite [55,56].

Direct charge transfer in the composites C1 and C2 is supported by the appearance of the additional absorption band, albeit weak, with the onset at 800 nm (Fig. 5d) [57,58]. DFT calculations also predicted Bader charge shift between flavin F3 and K-PHI of 0.023 electrons (see ESI for computational details).

Transient photocurrent measurements are indispensable to investigate light response properties of semiconductors, such as K-PHI [59,60]. Such measurements are typically done by immersing an electrode (typically FTO glass) coated with the analyzed material into the aqueous electrolyte. However, this approach was not suitable for the studied materials. Due to partial solubility of flavins in water, the coated FTO glass is not stable. Binders, such as PVDF, gave stable electrodes, but conductivity was too low to record reliable data.

The solution was found employing thin layers of conductive hydrogel between the electrodes that serves as the electrolyte (Figs. 6 and S21–22, see experimental procedure for details of the device fabrication). The developed architecture allows preserving the morphology of the analyzed material for hours due to low diffusion of the flavins into the bulk of the hydrogel. Compact size, thickness of only 10 mm, absence of electrolyte leakage and good light permeability are additional advantages of the fabricated device. The photoelectrodes in such architecture are stable for at least few hours (Fig. S23).

With the electrochemical device in hands, we performed different electrochemical tests: illuminated open circuit potential (OCP), linear sweep voltammetry (LSV), chronoamperometry (CA) and chronopotentiometry (CP) (Figs. 6 and S24).

Thus, illuminated OCP experiment showed a negative shift suggesting that all tested materials possess n-type conductivity, [61] while in CA experiments a positive photocurrent densities of 2–22 μA cm^{-2} were registered. Therefore, once irradiated, materials resistance decreases due to increase of charge carriers concentration. For pure K-PHI and its composites, these findings are in agreement with the reported earlier positive slope in the Mott-Schottky plot [62]. However, to the best of our knowledge, there is no data for flavins in solid state. The amplitude of the OCP change increases in the sequence K-PHI ≈ flavin < composite (Fig. S25) due to the introduction of the additional light absorber, a flavin ($\lambda_{onset} \leq 540$ nm).

Analysis of the CA data (Fig. S26) reveals that pure K-PHI shows higher photocurrent densities compared to pure flavins. At the same time, composite C1 shows twice higher photocurrent compared to pure K-PHI and 14 times higher photocurrent compared to pure flavin F1, supporting existence of charge transfer between the two components of the composite. Composites C2 and C3, however, showed lower photocurrents compared to the individual components. Analysis of absolute current densities (Fig. S27) suggests that surface properties of the photoelectrode have clear impact on the overall conductivity. Thus, K-PHI (hydrophilic), the flavin F1 (partially soluble in water) and their composite C1 show not only the highest photocurrent, but also the highest dark current in the series of studied materials. On the other hand, the flavin F2 (large hydrophobic molecule due to presence of multiple Br atoms) and its composite show the lowest dark current.

Since a Z-scheme relies on the excitation of both the composite components (K-PHI and flavin), here with two photons with different wavelength (due to different optical band gaps), we investigated the photocatalytic properties of the prepared composites under white light irradiation in a gas-solid batch photoreactor. We selected the photocatalytic CO_2 reduction reaction using water vapor as the electron and proton donor (see Fig. S28 for the detailed mechanism). We monitored the formation of CO, CH_4, MeOH and EtOH – common products of CO_2 reduction. In addition, no H_2 formed due to the fact that the investigated system is free of transition metal co-catalyst, which otherwise would facilitates hydrogen evolution.

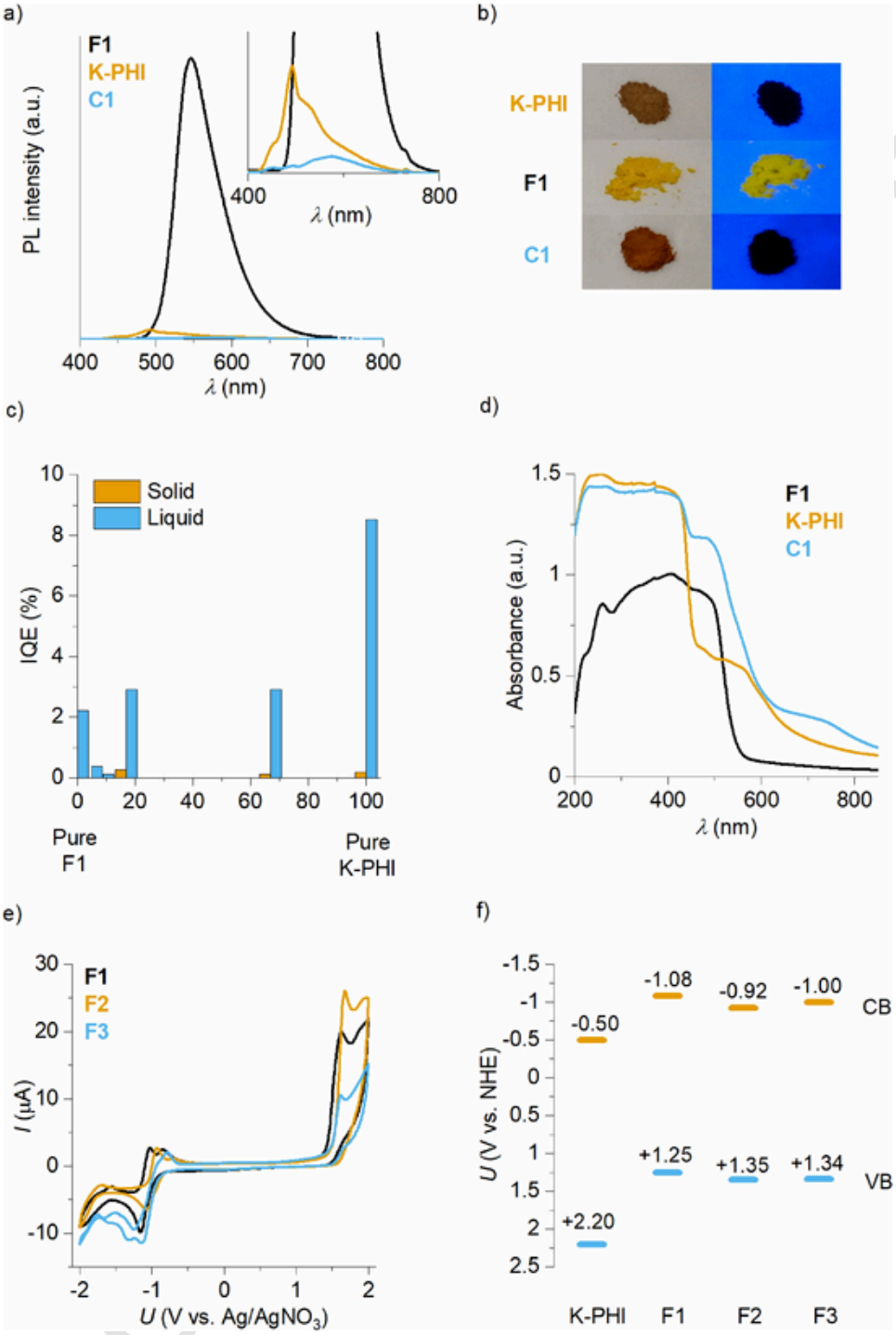

Fig. 5. Optical properties of flavins and composites. a) Solid state PL spectra of F1, K-PHI and the composite C1. Inset shows magnified PL spectra of K-PHI and the composite C1. b) Powder of K-PHI, flavin F1 and the composite C1 under ambient day light and under 365 nm irradiation. c) IQE of composites in solid state and dispersions in DMSO. X-axis represents K-PHI content. d) DRUV-vis absorption spectra of F1, K-PHI and composite C1. e) CV curves recorded using 2 mM solution of flavin in MeCN. Glassy carbon (diameter 3 mm) was used as a working electrode (WE), Ag wire in $AgNO_3$ (0.01 M) with $(nBu)_4N^+ClO_4^-$ (0.1 M) in MeCN – as a reference electrode (RE) and Pt wire – as a counter electrode (CE). f) CB and VB potentials of K-PHI are taken from the literature. [41] For flavins, CB and VB refer to HOMO and LUMO potentials determined from CV curves (Fig. 5e).

Fig. 7 shows the yield of the products obtained using pure K-PHI, flavins and their composites. Pure K-PHI and flavins F1 and F2 show selectivity toward alcohols, methanol and ethanol.

The same trend is conserved in the composites. Therefore, reduction selectivity of the composite is largely defined by the property of the incorporated flavin. Thus, considering photocatalytic reduction of CO_2 to CH_4, the productivity of the composite C3 is 15 % higher compared to the flavin F3, while composite C2 showed 2.5 times higher activity compared to the flavin F2. On the other hand, the productivity of photocatalytic reduction to CO can be increased by 27 % employing composite C2 compared to flavin F2 and 3 times using composite C3 compared to flavin F3.

Thermal response measurements recording the temperature of the materials during adsorption were conducted to probe the interaction of

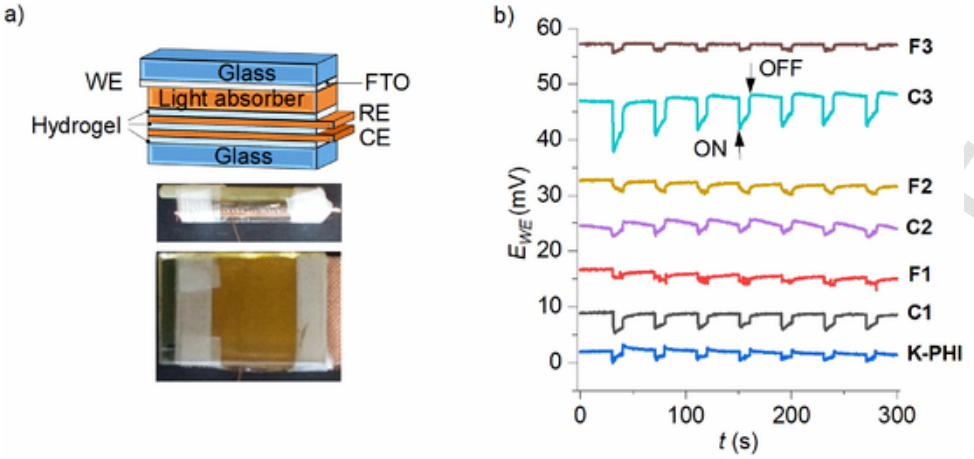

Fig. 6. Electrochemical measurements. a) Representative scheme of the electrochemical cell employing hydrogel layers as the electrolyte. Schematic representation, side and front views of the ready device; b) Illuminated OCP experiment. The experiment was performed in dark (30 s) followed by irradiation with white LED (10 s, 467 mW cm^{-2}). Seven cycles were recorded for each material. The temperature was kept at 25–30 °C by using air fan. Geometric area of the working electrode was 3.2 cm^2.

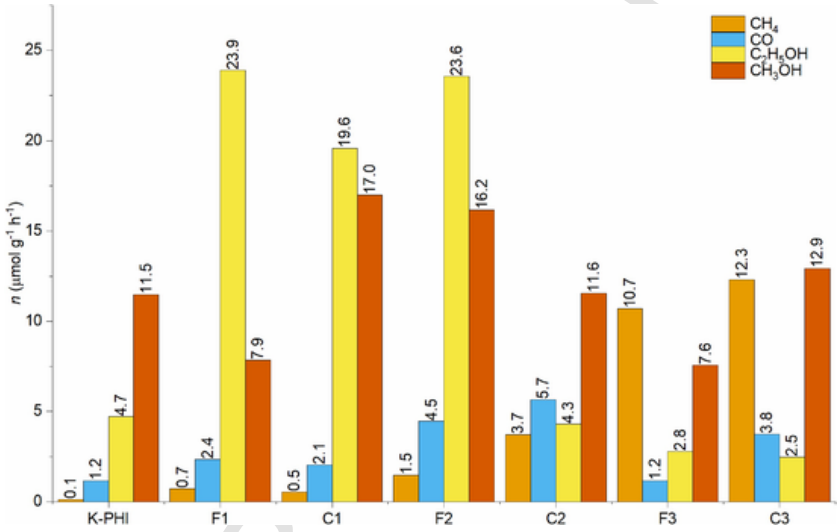

Fig. 7. Photocatalytic CO_2 reduction experiments comparing different catalysts.

CO_2 and H_2O with the surface of K-PHI, flavin F1 and the composite C1, as an example, (Figs. S29 and S30) [63]. Dry CO_2 has very low affinity to these materials (Fig. S31). When CO_2 saturated with water vapor at room temperature, significantly more heat is released due to additional adsorption of water. When helium instead of CO_2 is used as a carrier gas exemplarily for composite C1, the individual contribution of water adsorption can be estimated. The heat released is far less than in the presence of CO_2 and the difference is much larger than the contribution from dry CO_2 adsorption. Therefore, water vapor serves not only as electron and proton donor in the photocatalytic CO_2 reduction, it also enhances adsorption of CO_2 at the photocatalyst surface. Furthermore, adsorption of CO_2 and H_2O at the composite C1 is defined by the surface properties of K-PHI rather than flavin F1, as the integrated peak area is comparable to that of pure K-PHI, which gives another factor for the activity of the core-shell structure of the composite with K-PHI particles outside. However, the total amount of CO_2 molecules converted by the composite C1 is similar to that of the flavin F1 (Fig. S32), while CO_2 shows relatively weak affinity, implying that the band structure of the flavin determines the rate of the overall photocatalytic activity and selectivity towards a certain product.

From the results of photocatalytic tests, we conclude that selectivity of CO_2 photocatalytic reduction can be tuned by using composites of K-PHI and flavins. The forged Z-scheme heterojuntion between K-PHI and flavins provides a material with the reducing properties of pure flavin and oxidative properties of pure K-PHI. This phenomena, combined with longer life-times of excited states due to interface charge recombination, promotes the improvement of photocatalytic activities, compared to pure flavins [64,65].

4. Conclusions

In this work, three structurally different core-shell composites constructed from micro-sized crystals of flavin (the core) and decorated with K-PHI nanoparticles (the shell) have been prepared by a simple and straightforward co-precipitation/stabilization approach. The properties of the composites were investigated by SEM, XRD, TEM, EDX, IR and PL, while the results suggest formation of a spontaneous heterojunction between the core and the shell. The photocatalytic activity of the composites has been evaluated in reduction of CO_2 to CO, CH_4, MeOH and EtOH. The results suggest that the selectivity of the composites toward specific products is largely defined by flavins, i.e. the flavins constitute the reduction side. The K-PHI shell presumably promotes the liberation of oxygen by its very positive HOMO, accelerates the reaction, and changes the product distribution presumably by kinetic effects. Given the simplicity of flavins and carbon nitride synthe-

sis, the presented approach can lay a foundation for the construction of a library of composites for task-specific applications in serious uphill photocatalysis. Photoelectrochemical performance of flavins powder and their composites have been investigated using a dedicated electrochemical device employing a thin layer of conductive hydrogel as polymer electrolyte. In particular, a riboflavintetracetate-based composite showed a photocurrent two times higher than that of pure K-PHI and 14 times higher than pure riboflavintetracetate, suggesting higher charge mobility.

CRediT authorship contribution statement

Stefano Mazzanti: Conceptualization, Validation, Formal analysis, Investigation, Resources, Data curation, Writing - original draft, Visualization, Supervision, Project administration, Funding acquisition. **Shaowen Cao:** Conceptualization, Validation, Formal analysis, Investigation, Resources, Data curation, Writing - original draft, Visualization, Supervision, Project administration, Funding acquisition. **Katharina ten Brummelhuis:** Conceptualization, Validation, Formal analysis, Investigation, Resources, Data curation, Writing - original draft, Visualization, Supervision, Project administration, Funding acquisition. **Jagadish Khamrai:** Conceptualization, Validation, Formal analysis, Investigation, Resources, Data curation, Writing - original draft, Visualization, Supervision, Project administration, Funding acquisition. **Dmitry I. Sharapa:** Conceptualization, Validation, Formal analysis, Investigation, Resources, Data curation, Writing - original draft, Visualization, Supervision, Project administration, Funding acquisition. **Sol Youk:** Conceptualization, Validation, Formal analysis, Investigation, Resources, Data curation, Writing - original draft, Visualization, Supervision, Project administration, Funding acquisition. **Tobias Heil:** Conceptualization, Validation, Formal analysis, Investigation, Resources, Data curation, Writing - original draft, Visualization, Supervision, Project administration, Funding acquisition. **Nadezda V. Tarakina:** Conceptualization, Validation, Formal analysis, Investigation, Resources, Data curation, Writing - original draft, Visualization, Supervision, Project administration, Funding acquisition. **Volker Strauss:** Conceptualization, Validation, Formal analysis, Investigation, Resources, Data curation, Writing - original draft, Visualization, Supervision, Project administration, Funding acquisition. **Indrajit Ghosh:** Conceptualization, Validation, Formal analysis, Investigation, Resources, Data curation, Writing - original draft, Visualization, Supervision, Project administration, Funding acquisition. **Burkhard König:** Conceptualization, Validation, Formal analysis, Investigation, Resources, Data curation, Writing - original draft, Visualization, Supervision, Project administration, Funding acquisition. **Martin Oschatz:** Conceptualization, Validation, Formal analysis, Investigation, Resources, Data curation, Writing - original draft, Visualization, Supervision, Project administration, Funding acquisition. **Markus Antonietti:** Conceptualization, Validation, Formal analysis, Investigation, Resources, Data curation, Writing - original draft, Visualization, Supervision, Project administration, Funding acquisition. **Aleksandr Savateev:** Conceptualization, Validation, Formal analysis, Investigation, Resources, Data curation, Writing - original draft, Visualization, Supervision, Project administration, Funding acquisition.

Declaration of Competing Interest

The authors report no declarations of interest.

Acknowledgements

SM, AS and MA gratefully acknowledge Max Planck Society for financial support. JK, IG and BK thank the German Science Foundation (DFG, KO 1537/18-1) for financial support.

Appendix B. Supplementary data

Supplementary material related to this article can be found, in the online version, at doi:https://doi.org/10.1016/j.apcatb.2020.119773.

References

[1] C.D. Windle, R.N. Perutz, Advances in molecular photocatalytic and electrocatalytic CO2 reduction, Coord. Chem. Rev. 256 (2012) 2562–2570, doi:10.1016/j.ccr.2012.03.010.
[2] B. AlOtaibi, S. Fan, D. Wang, J. Ye, Z. Mi, Wafer-level artificial photosynthesis for CO2 reduction into CH4 and CO using GaN nanowires, ACS Catal. 5 (2015) 5342–5348, doi:10.1021/acscatal.5b00776.
[3] J. Qin, S. Wang, H. Ren, Y. Hou, X. Wang, Photocatalytic reduction of CO2 by graphitic carbon nitride polymers derived from urea and barbituric acid, Appl. Catal. B 179 (2015) 1–8, doi:10.1016/j.apcatb.2015.05.005.
[4] S. Gao, B. Gu, X. Jiao, Y. Sun, X. Zu, F. Yang, W. Zhu, C. Wang, Z. Feng, B. Ye, Y. Xie, Highly efficient and exceptionally durable CO2 photoreduction to methanol over freestanding defective single-unit-cell bismuth vanadate layers, J. Am. Chem. Soc. 139 (2017) 3438–3445, doi:10.1021/jacs.6b11263.
[5] W. Dai, J. Yu, Y. Deng, X. Hu, T. Wang, X. Luo, Facile synthesis of MoS2/Bi2WO6 nanocomposites for enhanced CO2 photoreduction activity under visible light irradiation, Appl. Surf. Sci. 403 (2017) 230–239, doi:10.1016/j.apsusc.2017.01.171.
[6] J.L. White, M.F. Baruch, J.E. Pander Iii, Y. Hu, I.C. Fortmeyer, J.E. Park, T. Zhang, K. Liao, J. Gu, Y. Yan, T.W. Shaw, E. Abelev, A.B. Bocarsly, Light-driven heterogeneous reduction of carbon dioxide: photocatalysts and photoelectrodes, Chem. Rev. 115 (2015) 12888–12935, doi:10.1021/acs.chemrev.5b00370.
[7] K.A. Ahrendt, C.J. Borths, D.W.C. MacMillan, New strategies for organic catalysis: the first highly enantioselective organocatalytic diels - Alder reaction, J. Am. Chem. Soc. 122 (2000) 4243–4244, doi:10.1021/ja000092s.
[8] T. Hering, B. Muhldorf, R. Wolf, B. Konig, Halogenase-inspired oxidative chlorination using flavin photocatalysis, Angew. Chem. Int. Ed. Engl. 55 (2016) 5342–5345, doi:10.1002/anie.201600783.
[9] B. Mühldorf, R. Wolf, Visible-light-driven aerobic photooxidation of aldehydes to methyl esters catalyzed by riboflavin tetraacetate, ChemCatChem 9 (2017) 920–923, doi:10.1002/cctc.201601504.
[10] J. Dad'ová, E. Svobodová, M. Sikorski, B. König, R. Cibulka, Photooxidation of sulfides to sulfoxides mediated by tetra-O-acetylriboflavin and visible light, ChemCatChem 4 (2012) 620–623, doi:10.1002/cctc.201100372.
[11] G. de Gonzalo, M.W. Fraaije, Recent developments in flavin-based catalysis, ChemCatChem 5 (2013) 403–415, doi:10.1002/cctc.201200466.
[12] P. Dongare, I. MacKenzie, D. Wang, D.A. Nicewicz, T.J. Meyer, Oxidation of alkyl benzenes by a flavin photooxidation catalyst on nanostructured metal-oxide films, Proc. Natl. Acad. Sci. U. S. A. 114 (2017) 9279–9283, doi:10.1073/pnas.1707318114.
[13] S.J.S. Düsel, B. König, Visible-light-mediated nitration of protected anilines, J. Org. Chem. 83 (2018) 2802–2807, doi:10.1021/acs.joc.7b03260.
[14] H. Iida, Y. Imada, S.I. Murahashi, Biomimetic flavin-catalysed reactions for organic synthesis, Org. Biomol. Chem. 13 (2015) 7599–7613, doi:10.1039/C5OB00854A.
[15] R. Lechner, S. Kummel, B. Konig, Visible light flavin photo-oxidation of methylbenzenes, styrenes and phenylacetic acids, Photochem. Photobiol. Sci. 9 (2010) 1367–1377, doi:10.1039/C0PP00202J.
[16] J.B. Metternich, R. Gilmour, One photocatalyst, n activation modes strategy for cascade catalysis: emulating coumarin biosynthesis with (-)-riboflavin, J. Am. Chem. Soc. 138 (2016) 1040–1045, doi:10.1021/jacs.5b12081.
[17] V. Mojr, E. Svobodova, K. Strakova, T. Nevesely, J. Chudoba, H. Dvorakova, R. Cibulka, Tailoring flavins for visible light photocatalysis: organocatalytic [2 + 2] cycloadditions mediated by a flavin derivative and visible light, Chem. Commun. (Cambridge, U. K.) 51 (2015) 12036–12039, doi:10.1039/C5CC01344E.
[18] N. Jürgensen, M. Ackermann, T. Marszalek, J. Zimmermann, A.J. Morfa, W. Pisula, U.H.F. Bunz, F. Hinkel, G. Hernandez-Sosa, Solution-processed Bio-OLEDs with a vitamin-derived riboflavin tetrabutyrate emission layer, ACS Sustain. Chem. Eng. 5 (2017) 5368–5372, doi:10.1021/acssuschemeng.7b00675.
[19] B. König, S. Kümmel, R. Cibulka, in: B. König (Ed.), Chemical Photocatalysis, 2013 De Gruyter, Berlin, Ch. 4., doi:10.1515/9783110269246.
[20] Z. Chen, A. Savateev, S. Pronkin, V. Papaefthimiou, C. Wolff, M.G. Willinger, E. Willinger, D. Neher, M. Antonietti, D. Dontsova, "The easier the better" preparation of efficient photocatalysts-metastable poly(heptazine imide) salts, Adv. Mater. 29 (2017), doi:10.1002/adma.201700555.
[21] A. Savateev, M. Antonietti, Heterogeneous organocatalysis for photoredox chemistry, ACS Catal. 8 (2018) 9790–9808, doi:10.1021/acscatal.8b02595.
[22] A. Savateev, M. Antonietti, Ionic carbon nitrides in solar hydrogen production and organic synthesis: exciting chemistry and economic advantages, ChemCatChem (2019), doi:10.1002/cctc.201901076.
[23] A. Savateev, I. Ghosh, B. König, M. Antonietti, Photoredox catalytic organic transformations using heterogeneous carbon nitrides, Angew. Chem. Int. Ed. Engl. (2018) 15936–15947, doi:10.1002/anie.201802472.

[24] I. Ghosh, J. Khamrai, A. Savateev, N. Shlapakov, M. Antonietti, B. König, Organic semiconductor photocatalyst can bifunctionalize arenes and heteroarenes, Science 365 (2019) 360–366, doi:10.1126/science.aaw3254.
[25] Y. Cai, Y. Tang, L. Fan, Q. Lefebvre, H. Hou, M. Rueping, Heterogeneous visible-light photoredox catalysis with graphitic carbon nitride for α-aminoalkyl radical additions, allylations, and heteroarylations, ACS Catal. 8 (2018) 9471–9476, doi:10.1021/acscatal.8b02937.
[26] C. Cavedon, A. Madani, P.H. Seeberger, B. Pieber, Semiheterogeneous dual nickel/photocatalytic (Thio)etherification using carbon nitrides, Org. Lett. 21 (2019) 5331–5334, doi:10.1021/acs.orglett.9b01957.
[27] C. Yang, R. Li, K.A.I. Zhang, W. Lin, K. Landfester, X. Wang, Heterogeneous photoredox flow chemistry for the scalable organosynthesis of fine chemicals, Nat. Commun. 11 (2020) 1239, doi:10.1038/s41467-020-14983-w.
[28] L. Möhlmann, S. Blechert, Carbon nitride-catalyzed photoredox sakurai reactions and allylborations, Adv. Synth. Catal. 356 (2014) 2825–2829, doi:10.1002/adsc.201400551.
[29] Y. Markushyna, C.A. Smith, A. Savateev, Organic photocatalysis: carbon nitride semiconductors vs, Mol. Catal., Eur. J. Org. Chem. (2019), doi:10.1002/ejoc.201901112.
[30] S. Cao, J. Low, J. Yu, M. Jaroniec, Polymeric photocatalysts based on graphitic carbon nitride, Adv. Mater. 27 (2015) 2150–2176, doi:10.1002/adma.201500033.
[31] A. Savateev, S. Pronkin, J.D. Epping, M.G. Willinger, M. Antonietti, D. Dontsova, Synthesis of an electronically modified carbon nitride from a processable semiconductor, 3-amino-1,2,4-triazole oligomer: via a topotactic-like phase transition, J. Mater. Chem. A 5 (2017) 8394–8401, doi:10.1039/C7TA01714F.
[32] J. Barrio, M. Shalom, Rational design of carbon nitride materials by supramolecular preorganization of monomers, ChemCatChem 10 (2018) 5573–5586, doi:10.1002/cctc.201801410.
[33] A. Savateev, D. Dontsova, B. Kurpil, M. Antonietti, Highly crystalline poly(heptazine imides) by mechanochemical synthesis for photooxidation of various organic substrates using an intriguing electron acceptor – elemental sulfur, J. Catal. 350 (2017) 203–211, doi:10.1016/j.jcat.2017.02.029.
[34] Z. Chen, A. Savateev, S. Pronkin, V. Papaefthimiou, C. Wolff, M.G. Willinger, E. Willinger, D. Neher, M. Antonietti, D. Dontsova, "The easier the better" preparation of efficient photocatalysts—Metastable poly(heptazine imide) salts, Adv. Mater. 29 (2017) 1700555, doi:10.1002/adma.201700555.
[35] G. Zhang, G. Li, Z.A. Lan, L. Lin, A. Savateev, T. Heil, S. Zafeiratos, X. Wang, M. Antonietti, Optimizing optical absorption, exciton dissociation, and charge transfer of a polymeric carbon nitride with ultrahigh solar hydrogen production activity, Angew. Chem. Int. Ed. Engl. 56 (2017) 13445–13449, doi:10.1002/anie.201706870.
[36] Z. Xu, C. Zhuang, Z. Zou, J. Wang, X. Xu, T. Peng, Enhanced photocatalytic activity by the construction of a TiO2/carbon nitride nanosheets heterostructure with high surface area via direct interfacial assembly, Nano Res. 10 (2017) 2193–2209, doi:10.1007/s12274-017-1453-2.
[37] J. Byun, W. Huang, D. Wang, R. Li, K.A.I. Zhang, CO2 -triggered switchable hydrophilicity of a heterogeneous conjugated polymer photocatalyst for enhanced catalytic activity in water, Angew. Chem. Int. Ed. Engl. 57 (2018) 2967–2971, doi:10.1002/anie.201711773.
[38] C. Yang, B.C. Ma, L. Zhang, S. Lin, S. Ghasimi, K. Landfester, K.A. Zhang, X. Wang, Molecular engineering of conjugated polybenzothiadiazoles for enhanced hydrogen production by photosynthesis, Angew. Chem. Int. Ed. Engl. 55 (2016) 9202–9206, doi:10.1002/anie.201603532.
[39] Z.A. Lan, G. Zhang, X. Chen, Y. Zhang, K.A.I. Zhang, X. Wang, Reducing the exciton binding energy of donor-acceptor-Based conjugated polymers to promote charge-induced reactions, Angew. Chem. Int. Ed. Engl. 58 (2019) 10236–10240, doi:10.1002/anie.201904904.
[40] G. Zhang, L. Lin, G. Li, Y. Zhang, A. Savateev, S. Zafeiratos, X. Wang, M. Antonietti, Ionothermal synthesis of triazine-heptazine-based copolymers with apparent quantum yields of 60 % at 420 nm for solar hydrogen production from "sea water", Angew. Chem. Int. Ed. Engl. 57 (2018) 9372–9376, doi:10.1002/anie.201804702.
[41] A. Savateev, B. Kurpil, A. Mishchenko, G. Zhang, M. Antonietti, A "waiting" carbon nitride radical anion: a charge storage material and key intermediate in direct C-H thiolation of methylarenes using elemental sulfur as the "S"-source, Chem. Sci. 9 (2018) 3584–3591, doi:10.1039/C8SC00745D.
[42] S. Mazzanti, B. Kurpil, B. Pieber, M. Antonietti, A. Savateev, Dichloromethylation of enones by carbon nitride photocatalysis, Nat. Commun. 11 (2020) 1387, doi:10.1038/s41467-020-15131-0.
[43] A. Savateev, N.V. Tarakina, V. Strauss, T. Hussain, K. Ten Brummelhuis, J.M. Sanchez Vadillo, Y. Markushyna, S. Mazzanti, A.P. Tyutyunnik, R. Walczak, M. Oschatz, D. Guldi, A. Karton, M. Antonietti, Potassium poly(Heptazine imide) - transition metal-free solid state triplet sensitizer in cascade energy transfer and [3 + 2]-cycloadditions, Angew. Chem. Int. Ed. Engl. 59 (2020) 15061–15068, doi:10.1002/anie.202004747.
[44] H. Schlomberg, J. Kroger, G. Savasci, M.W. Terban, S. Bette, I. Moudrakovski, V. Duppel, F. Podjaski, R. Siegel, J. Senker, R.E. Dinnebier, C. Ochsenfeld, B.V. Lotsch, Structural insights into poly(Heptazine imides): a light-storing carbon nitride material for dark photocatalysis, Chem. Mater. 31 (2019) 7478–7486, doi:10.1021/acs.chemmater.9b02199.
[45] Y. Markushyna, C. Teutloff, B. Kurpil, D. Cruz, I. Lauermann, Y. Zhao, M. Antonietti, A. Savateev, Halogenation of aromatic hydrocarbons by halide anion oxidation with poly(heptazine imide) photocatalyst, Appl. Catal. B 248 (2019) 211–217, doi:10.1016/j.apcatb.2019.02.016.
[46] Y. Markushyna, P. Lamagni, C. Teutloff, J. Catalano, N. Lock, G. Zhang, M. Antonietti, A. Savateev, Green radicals of potassium poly(heptazine imide) using light and benzylamine, J. Mater. Chem. A 7 (2019) 24771–24775, doi:10.1039/C9TA09500D.
[47] B. Kurpil, A. Savateev, V. Papaefthimiou, S. Zafeiratos, T. Heil, S. Özenler, D. Dontsova, M. Antonietti, Hexaazatriphenylene doped carbon nitrides—biomimetic photocatalyst with superior oxidation power, Appl. Catal. B: Environ. 217 (2017) 622–628, doi:10.1016/j.apcatb.2017.06.036.
[48] B. Kurpil, K. Otte, A. Mishchenko, P. Lamagni, W. Lipiński, N. Lock, M. Antonietti, A. Savateev, Carbon nitride photocatalyzes regioselective aminium radical addition to the carbonyl bond and yields N-fused pyrroles, Nat. Commun. 10 (2019) 945-945, doi:10.1038/s41467-019-08652-w.
[49] B. Kurpil, K. Otte, M. Antonietti, A. Savateev, Photooxidation of N-acylhydrazones to 1,3,4-oxadiazoles catalyzed by heterogeneous visible-light-active carbon nitride semiconductor, Appl. Catal. B 228 (2018) 97–102, doi:10.1016/j.apcatb.2018.01.072.
[50] B. Kurpil, Y. Markushyna, A. Savateev, Visible-light-driven reductive (cyclo)dimerization of chalcones over heterogeneous carbon nitride photocatalyst, ACS Catal. 9 (2019) 1531–1538, doi:10.1021/acscatal.8b04182.
[51] A.M. Díez-Pascual, D. García-García, M.P. San Andrés, S. Vera, Determination of riboflavin based on fluorescence quenching by graphene dispersions in polyethylene glycol, RSC Adv. 6 (2016) 19686–19699, doi:10.1039/C5RA25547C.
[52] Y. Chen, J.W.Y. Lam, R.T.K. Kwok, B. Liu, B.Z. Tang, Aggregation-induced emission: fundamental understanding and future developments, Mater. Horiz. 6 (2019) 428–433, doi:10.1039/C8MH01331D.
[53] A.B. Jorge, D.J. Martin, M.T.S. Dhanoa, A.S. Rahman, N. Makwana, J. Tang, A. Sella, F. Corà, S. Firth, J.A. Darr, P.F. McMillan, H2 and O2 evolution from water half-splitting reactions by graphitic carbon nitride materials, J. Phys. Chem. C 117 (2013) 7178–7185, doi:10.1021/jp4009338.
[54] W. Yu, D. Xu, T. Peng, Enhanced photocatalytic activity of g-C3N4 for selective CO2 reduction to CH3OH via facile coupling of ZnO: a direct Z-scheme mechanism, J. Mat. Chem. A 3 (2015) 19936–19947, doi:10.1039/C5TA05503B.
[55] Z. Pan, G. Zhang, X. Wang, Polymeric carbon nitride/reduced graphene Oxide/Fe2 O3: all-solid-State Z-Scheme system for photocatalytic overall water splitting, Angew. Chem. Int. Ed. Engl. 58 (2019) 7102–7106, doi:10.1002/ange.201902634.
[56] L. Zhao, X. Chen, X. Wang, Y. Zhang, W. Wei, Y. Sun, M. Antonietti, M.M. Titirici, One-step solvothermal synthesis of a carbon@TiO(2) dyade structure effectively promoting visible-light photocatalysis, Adv. Mater. 22 (2010) 3317–3321, doi:10.1002/adma.201000660.
[57] K.S. Iyer, C.L. Raston, M. Saunders, Hierarchical aqueous self-assembly of C60 nano-whiskers and C60-silver nano-hybrids under continuous flow, Lab Chip 7 (2007) 1121–1124, doi:10.1039/B707037C.
[58] Y. Li, Z. Wang, T. Xia, H. Ju, K. Zhang, R. Long, Q. Xu, C. Wang, L. Song, J. Zhu, J. Jiang, Y. Xiong, Implementing metal-to-Ligand charge transfer in organic semiconductor for improved visible-near-Infrared photocatalysis, Adv. Mater. 28 (2016) 6959–6965, doi:10.1002/adma.201601960.
[59] F. Le Formal, K. Sivula, M. Grätzel, The transient photocurrent and photovoltage behavior of a hematite photoanode under working conditions and the influence of surface treatments, J. Phys. Chem. 116 (2012) 26707–26720, doi:10.1021/jp308591k.
[60] R.C.I. MacKenzie, C.G. Shuttle, M.L. Chabinyc, J. Nelson, Extracting microscopic device parameters from transient photocurrent measurements of P3HT:PCBM solar cells, Adv. Energy Mat. 2 (2012) 662–669, doi:10.1002/aenm.201100709.
[61] Z. Chen, H.N. Dinh, E. Miller, Photoelectrochemical Water Splitting, Standards, Experimental Methods and Protocols, Springer, 2013, doi:10.1007/978-1-4614-8298-7_5.
[62] D. Dontsova, S. Pronkin, M. Wehle, Z. Chen, C. Fettkenhauer, G. Clavel, M. Antonietti, Triazoles: a new class of precursors for the synthesis of negatively charged carbon nitride derivatives, Chem. Mat. 27 (2015) 5170–5179, doi:10.1021/acs.chemmater.5b00812.
[63] M. Oschatz, M. Leistner, W. Nickel, S. Kaskel, Advanced structural analysis of nanoporous materials by thermal response measurements, Langmuir 31 (2015) 4040–4047, doi:10.1021/acs.langmuir.5b00490.
[64] D.M. Arias-Rotondo, J.K. McCusker, The photophysics of photoredox catalysis: a roadmap for catalyst design, Chem. Soc. Rev. 45 (2016) 5803–5820, doi:10.1039/C6CS00526H.
[65] S.S. Meryem, S. Nasreen, M. Siddique, R. Khan, An overview of the reaction conditions for an efficient photoconversion of CO2, Rev. Chem. Eng. 34 (2018) 409–425, doi:10.1515/revce-2016-0016.